Hygrothermoelastic analysis of non-simple nano-beam induced by ramp-type heating

Article *in* Archive of Applied Mechanics · May 2023

DOI: 10.1007/s00419-023-02444-x

3 authors:

Nagesh Dipak Dhore
GRAMGEETA MAHAVIDYALAYA CHIMUR
2 PUBLICATIONS **0** CITATIONS
SEE PROFILE

Lalsingh Khalsa
MG COLLEGE ARMORI
79 PUBLICATIONS **215** CITATIONS
SEE PROFILE

Vinod Varghese
S.S.R. Bharti Science College, Arni, Yavatmal, India
133 PUBLICATIONS **254** CITATIONS
SEE PROFILE

Archive of Applied Mechanics
https://doi.org/10.1007/s00419-023-02444-x

ORIGINAL

Nagesh Dhore · Lalsingh Khalsa · Vinod Varghese

Hygrothermoelastic analysis of non-simple nano-beam induced by ramp-type heating

Received: 25 January 2023 / Accepted: 9 May 2023

Abstract This study investigates a two-temperature hygrothermoelastic model to describe the effects of coupled temperature and moisture in a non-simple nano-beam subjected to hygrothermal loading. This paper analyses the hygrothermal distribution of an Euler–Bernoulli beam with a rectangular cross-section beam. A closed-form solution for temperature, moisture, displacement and hygrothermal stresses is obtained using the decoupling and integral transform methods along the thickness direction. A numerical example with porous composite material in the picoseconds scale has been calculated to illustrate the effect of the ramping time parameter within the hygrothermal field. The relevance of the influence of various characteristics is examined. The appropriate discussions and conclusions are reached.

Keywords Hygrothermoelasticity · Non-simple nano-beam · Finite Fourier transform · Euler–Bernoulli equation · Ramp-type heating

1 Introduction

Over the past two decades, scientific study has focused a lot on nanoscale structures because of their superior electrical and mechanical properties. Nano-structures are becoming increasingly valuable for scientists in various sectors, including sensor technology, composite materials, and electromechanical systems. It may be due to the hygrothermoelastic responses of composite nano-structures possessing many advantageous qualities [1]. But on the other extreme, the interactions between temperature, moisture, and thermoelastic deformation are more complicated during calculation. Many researchers have investigated the related hygrothermoelastic problems in this regard; however, just a few of those investigations may be listed here as a brief survey.

Using the integral transform approach, Chang and Weng [2] presented a linear hygrothermoelastic theory to analyze transient responses in various structures subjected to hygrothermal loading. Under the specified surface temperature and moisture load, Sugano [3] obtained analytical solutions for the heat and moisture equation and its associated hygrothermal stress in a functionally graded material plate. Chiba and Sugano [4] studied the heat and moisture equation in a multilayer plate subjected to hygrothermal loads. The effects of hygrothermal loading on the bending of two-dimensional, multilayered composite plates on Carrera's Unified Formulation framework were investigated by Brischetto [5]. Ishihara et al. [6] considered nonlinear

N. Dhore (✉)
Department of Mathematics, Gramgeeta Mahavidyalaya Chimur, Chandrapur, India
e-mail: nageshdhore@gmail.com

L. Khalsa · V. Varghese
Department of Mathematics, M.G. College, Armori, Gadchiroli, India
e-mail: lalsinghkhalsa@yahoo.com

V. Varghese
e-mail: vino7997@gmail.com

Published online: 26 May 2023

coupling while formulating and quantifying the hygrothermoelastic field in a porous medium subjected to heat and moisture loading. A functionally graded magnetoelectroelastic sphere subject to hygrothermal loading was explored by Saadatfar and Aghaie-Khafri [7]. Zenour [8] described the interplay of electric potentials, displacement, and elastic deformations to explain the hygrothermal reactions in inhomogeneous piezoelectric hollow cylinders subjected to mechanical stress and electric potential. Using the potential theory approach, Zhao et al. [9] developed a steady-state solution for three-dimensional hygrothermal media. Most previous works exposed the hygrothermal environment to the static and dynamic properties of composite or smart material constructions. To frame a model of two-temperature hygrothermoelastic diffusion theory for a non-simple rigid material, Sonal et al. [10] investigated the theoretical framework to couple both classical Fourier's and Fick's laws. They obtained solutions by employing a new integral transform technique.

Many authors have studied the effects of coupled temperature and moisture on the vibration in microstructures subjected to hygrothermal loading. Hosseinian et al. [11] analyzed the effect of hygrothermal conditions of microresonators, whereas Jan et al. [12] studied a resonator's frequency response in a hygrothermal environment by experimentation. Nguyen et al. [13] investigated the influence of a hygrothermal environment on a cantilever. Jouneghani et al. [14] investigated the effects of both heat and moisture on the bending behavior of porous, functionally graded nano-beams. Eichler et al. [15] discussed the nonlinear damping characteristics of carbon nano-tube and graphene resonators capable of achieving ultra-high-quality factors. Ebrahimi and Barati [16] used the nonlocal and strain gradient model to investigate the hygrothermal impacts on the buckling behavior of graphene sheets. Most of the studies mentioned above are based on Fourier's widely applied classical law. Kumar [17] investigated the thermoelastic damping of a microbeam resonator by employing three-phase-lag thermoelasticity. Yousef et al. [18] developed an analytical solution for a thermal model of a silicon microbeam resonator subjected to static stress using the Lord–Shulman and dual-phase-lag heat conduction models with fractional derivative. Zhang et al. [19] explored the time-fractional diffusion-wave equations introduced to represent a pipe's coupled temperature and moisture diffusion by separating variables and applying the Laplace transform.

In such conditions, as many researchers have noted, the classical Fourier law, which predicts an infinite propagation speed for thermal signals, is no longer applicable [20]. This paradox can be eliminated by the non-Fourier effect of heat conduction, which accounts for the impact of mean free time (thermal relaxation time) in the collision process of energy carriers. The conventional Fourier heat conduction theory is commonly applied to analyze microscale beams, whereas the non-Fourier heat conduction theory is rarely used. Some generalized diffusion or heat conduction models, such as the hyperbolic heat conduction model by Lord and Shulman [21], the dual-phase-lag diffusion model by Tzou [22], and the fractional diffusion models by Povstenko [23], have been developed to counteract the drawback. Sun et al. [24] studied the damping of microbeam resonators during pulsed laser heating in the context of generalized thermoelasticity with a single relaxation time. Soh [25] explored the non-Fourier effects on a microscale beam coupled with thermoelastic vibration with a laser pulse. Youssef and Elsibai [26] used the Green and Naghdi model to study the thermoelastic vibration response of a gold nano-beam resonator subjected to ramp-type heating.

Andarwa and Tabrizi [27] improved Luikov's heat and mass transfer model by including a relaxation time to characterize the phase lag of heat flux. This allowed them to handle hygrothermoelastic problems, which have a very limited amount of study that is based on generalized diffusion theories. Silva et al. [28] expanded the linear Luikov model with non-Markovian processes to study anomalous diffusion. Ezzat et al. [29] analyzed multi-field diffusion problems using the state-space method. El-Karamany and Ezzat [30] developed memory-dependent constitutive equations for anisotropic and isotropic thermoelastic diffusion. Using the meshless local Petrov–Galerkin method, Hosseini et al. [31] performed a two-dimensional investigation of linked non-Fick diffusion–thermoelasticity or so-called hygrothermoelasticity. Peng et al. [32] suggested a non-Fourier hyperbolic heat–moisture coupling model for analyzing the hygrothermoelastic responses of a cylinder subjected to various boundary conditions. Using the hyperbolic hygrothermal coupled model, Xue et al. [33] examined the crack problem of a hollow cylinder with a circumferential crack. Zhang et al. [34] developed a fractional coupling hygrothermoelastic model to investigate anomalous diffusion behaviors in heat and moisture transport processes. The initial research shows that the non-Fourier effects of heat and moisture diffusion coupling are observable and essential. It cannot be ignored, particularly for non-simple hygrothermoelastic media in nano-structures that have not yet been considered. To the author's knowledge, there haven't been any reports of a solution that uses the coupling of the classical Fourier's and Fick's laws to frame a two-temperature hygrothermoelastic model for non-simple nano-structures.

This manuscript attempts to determine a new non-simple hygrothermoelastic diffusion model by combining traditional Fourier's and Fick's equations inside a theoretical framework. Based on the hygrothermoelasticity

approach, a system of linearly linked partial differential equations for thermal and moisture diffusion in a non-simple nano-beam under a ramp-type temperature sectional heat supply is created. Lastly, an integral transform technique is used to develop closed-form formulas for temperature, moisture, vibration, and hygrothermal stresses for a rectangular nano-beam subjected to hydrothermal loading along the thickness direction.

2 Formulation of basic equation for non-simple thermal diffusion

The theory proposed by Henry [35] has suggested that small variations $\sigma = \partial M/\partial C$ and $\omega = -(\partial M/\partial T)$ are related to the mass of absorbed moisture as

$$M = \sigma C - \omega T + \text{constant} \tag{1}$$

in a unit mass of solid to the mass of moisture, C, in a unit volume of void space and the temperature, T, and to keep equations readily soluble, we assume σ and ω as constant to avoid mathematical complexity.

Now taking the rate of change of C in which mass of moisture is being absorbed or given off by the solid as $\gamma\,(\partial M/\partial t)$, where $\gamma = [(1-\alpha)/\alpha]\,\rho_s$, ρ_s is the true density of the solid, α is the ratio of the capacities for the diffusing material of equal volumes of the solid and the surrounding medium, D_1 is vapor diffusion coefficient under no-absorption condition, respectively. Then the equation for moisture diffusion is

$$\frac{\partial C}{\partial t} = D_1\,\nabla^2 C - \frac{1-\alpha}{\alpha}\rho_s \frac{\partial M}{\partial t}.$$

or

$$D_1\,\nabla^2 C = \frac{\partial C}{\partial t} + \gamma \frac{\partial M}{\partial t} \tag{2}$$

The rate of evolution of heat per unit volume is $k\rho'\,(\partial M/\partial t)$, where $\rho' = [(\rho-\rho_p)/(\rho_s-\rho_p)]\,\rho_s$ is the mass of solid per unit volume of the whole, ρ is the overall densities of the solid, ρ_p is the density of material filling the pores, and the equation for the thermal diffusion is

$$c_v\rho' \frac{\partial T}{\partial t} = \kappa\nabla^2 T + k\rho' \frac{\partial M}{\partial t}$$

Or

$$D_2\nabla^2 T = \frac{\partial T}{\partial t} - \varepsilon \frac{\partial M}{\partial t} \tag{3}$$

in which D_2 is the thermal diffusion coefficient under the condition of no absorption, $\varepsilon = k/c_v$, with k being the overall thermal conductivity of the material, c_v is the total calorific capacity, and $\kappa = k/c_v\rho$ is representing thermal diffusivity, respectively.

Substituting the value of M from Eqs. (1) in (2), one gets

$$D\nabla^2 C = \frac{\partial C}{\partial t} - \lambda \frac{\partial T}{\partial t} \tag{4}$$

where

$$D = \frac{D_1}{(\gamma\sigma+1)}, \lambda = \frac{\gamma\omega}{\gamma\sigma+1}. \tag{5}$$

Similarly, eliminating M from Eqs. (3) using (1), one obtains

$$\mathfrak{D}\nabla^2 T = \frac{\partial T}{\partial t} - \varphi \frac{\partial C}{\partial t} \tag{6}$$

where

$$\mathfrak{D} = \frac{D_2}{1+\varepsilon\omega}, \varphi = \frac{\varepsilon\sigma}{1+\varepsilon\omega}. \tag{7}$$

Here λ is the adiabatic coefficient, φ is isothermal coefficient, D is vapor diffusion coefficient under isothermal conditions, and $\mathfrak{D}$ is the thermal diffusion coefficient under the state of constant vapor concentration.

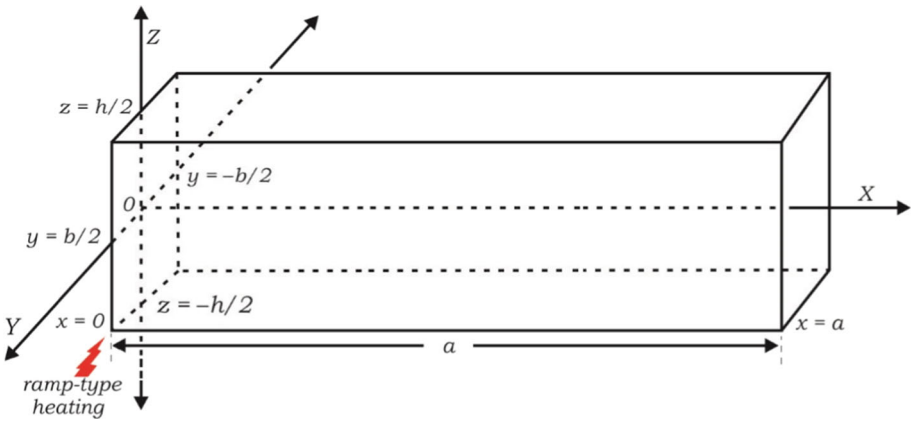

Fig. 1 Cross-sectional configuration of a rectangular beam

One of the non-classical thermoelasticity theories of elastic solids involves incorporating the two-temperature model. In this context, Chen and Gurtin [36] suggested classifying real materials into simple and non-simple materials by considering two temperatures, conductive and thermodynamic. According to the corresponding theory, unlike simple materials, where they are similar, the two temperatures were not the same for non-simple materials. Chen et al. [37] extended the investigations to deformable bodies and demonstrated that these materials contain an additional term involving the time derivative of the Laplacian of the conductive temperature, showing the relationship between the two temperatures by

$$\phi = T - d_T \nabla^2 T\,,\ d_T \geq 0 \tag{8}$$

in which ϕ is the thermodynamic temperature, T is the conductive temperature, and d_T is the temperature discrepancy factor. Thus, the thermodynamics and conductive temperatures are not identical for non-simple materials but identical for simple materials. The temperature discrepancy factor d_T, which distinguishes the two-temperature thermoelasticity theory from the classical approach, is crucial. Concerning the one-temperature generalized thermoelasticity theory, specifically in the limit as $d_T \to 0, \phi \to T$ those results in the classical theory. So, Eq. (6) can be expressed as follows for a non-simple medium as

$$\mathfrak{D}\left(1 + \frac{d_T}{k}\frac{\partial}{\partial t}\right)\nabla^2 T = \frac{\partial T}{\partial t} - \varphi\frac{\partial C}{\partial t} \tag{9}$$

Thus, Eqs. (4) and (9) are the system of linearly coupled partial differential equations.

3 Formulation of the problem

Consider a rectangular nano-beam with length $a\,(0 \leq x \leq a)$, cross section of width b $(-b/2 \leq y \leq b/2)$, and thickness c $(-c/2 \leq z \leq c/2)$ in a hygrothermal environment, as shown in Fig. 1.

We define the x-axis along the beam's axis and the y- and z-axes parallel to the dimensions' surfaces b and c, respectively. In equilibrium, the beam is unstrained, unstressed, and at temperature T_0 and moisture C_0 everywhere [38]. A displacement field $u_i\,(i = x, y, z)$, a temperature field $T = T_0 + \theta$, and moisture $C = C_0 + \psi$ all describe the beam's deviation from equilibrium. The displacement field u_i, the relative temperature change θ, and the moisture change ψ as well as the strain and stress tensors u_{ij}, and σ_{ij}, are all positions and time functions. Similarly, we consider pure transverse motion in the z-direction and use the standard Euler–Bernoulli assumption that any plane cross section, initially perpendicular to the axis of the beam, remains plane and perpendicular to the neutral surface throughout bending. The neutral surface is the surface that runs the entire length of the beam and experiences neither extension nor contraction during bending. Thus, the displacement components under the Euler–Bernoulli hypothesis may be assumed to be [24, 25]

$$u = -z\frac{\partial w(x,t)}{\partial x}, v = 0, w(x,y,z,t) = w(x,t) \tag{10}$$

where w is often called the transverse deflection of the beam.

The displacement components are given in Eq. (10), and in the presence of temperature and moisture, the constitutive equation of the one-dimensional version reads as

$$\frac{\sigma_x}{E} = -z\frac{\partial^2 w(x,t)}{\partial x^2} - [\alpha_1 (T - T_0) + \alpha_2 (C - C_0)] \tag{11}$$

in which α_1 and α_2 are the coefficients of linear thermal expansion and moisture absorption, $T - T_0$ is temperature change, and $C - C_0$ is moisture change, respectively.

The governing equation for the dynamics of the beam may be expressed in the form [39]

$$EI\frac{\partial^4 w}{\partial x^4} + \rho A\frac{\partial^2 w}{\partial t^2} + \frac{\partial^2 M_T}{\partial x^2} = 0 \tag{12}$$

subjected to clamped boundary conditions

$$w\,|_{t=0} = 0, \ \left.\frac{\partial w}{\partial t}\right|_{t=0} = 0, \tag{13}$$

$$w\,|_{x=0} = 0, \ w\,|_{x=a} = 0, \tag{14}$$

$$\left.\frac{\partial^2 w}{\partial x^2}\right|_{x=0} = 0, \ \left.\frac{\partial^2 w}{\partial x^2}\right|_{x=a} = 0, \tag{15}$$

where E is Young's modulus, $I = bh^3/12$ is the inertial moment about the y-axis, ρ is the density of the beam, $w = w(x, t)$ is the lateral deflection, x is the distance along the length of the beam, $A = bh$ is the cross-sectional area, t is the time, and M_c is the hygrothermal moment, given as [39]

$$M_c = bE\int_{-h/2}^{h/2} [\alpha_1 (T - T_0) + \alpha_2 (C - C_0)]\, z\, \mathrm{d}z \tag{16}$$

In particular, neglecting the effect of moisture ($\alpha_2 = 0$), a Fourier thermoelastic problem is recovered and studied in a research paper [36].

4 Solution of the problem

We assume that there is no flow of heat and moisture across the upper and lower surfaces of the beam, which equivalently requires vanishing temperature and moisture gradient on both surfaces so that [39]

$$\frac{\partial T}{\partial z} = \frac{\partial C}{\partial z} = 0, \quad z = \pm h/2, \ t > 0 \tag{17}$$

Moreover, since the length is much larger than the thickness for slender beams, temperature and moisture gradients in the cross-sectional area are much larger than the corresponding gradients along the longitudinal direction. We assume the temperature and moisture distribution along the thickness direction will vary in terms of a $\sin(gz)$, $g = \pi/h$ function.

$$T(x,z,t) = \theta(x,t)\sin(gz) \tag{18}$$

$$C(x,z,t) = \vartheta(x,t)\sin(gz) \tag{19}$$

Hence, using Eqs. (18) and (19) in Eqs. (4) and (9) gives

$$D\left(\frac{\partial^2 \vartheta}{\partial x^2} - g^2\vartheta\right) = \frac{\partial \vartheta}{\partial t} - \lambda\frac{\partial \theta}{\partial t} \tag{20}$$

$$\mathfrak{D}\left(1 + \frac{d_T}{k}\frac{\partial}{\partial t}\right)\left(\frac{\partial^2 \theta}{\partial x^2} - g^2\theta\right) = \frac{\partial \theta}{\partial t} - \varphi\frac{\partial \vartheta}{\partial t} \tag{21}$$

subjected to boundary conditions which are as follows:

$$\theta\,|_{t=0} = 0,\ \left.\frac{\partial\theta}{\partial t}\right|_{t=0} = 0, \tag{22}$$

$$\vartheta\,|_{t=0} = 0,\ \left.\frac{\partial\vartheta}{\partial t}\right|_{t=0} = 0, \tag{23}$$

$$\theta\,|_{x=0} = 0,\ \theta\,|_{x=a} = \begin{cases} \dfrac{\theta_1}{t_0}\,t & \text{for } 0 \le t \le t_0, \\ \theta_1 & \text{for } t \ge t_0, \end{cases} \tag{24}$$

$$\vartheta\,|_{x=0} = 0,\ \vartheta|_{x=a} = \begin{cases} \dfrac{\vartheta_1}{t_0}\,t & \text{for } 0 \le t \le t_0, \\ \vartheta_1 & \text{for } t \ge t_0, \end{cases} \tag{25}$$

where t_0 is a ramp-type parameter and θ_1 and ϑ_1 are both fixed constants.

Applying the Laplace transform technique [40] as defined by the formula

$$\overline{f}(s) = L[f(t)] = \int_0^\infty f(t)e^{-st}\mathrm{d}t,\ s > 0 \tag{26}$$

where s is the Laplace parameter.

Taking the Laplace transformation of Eqs. (20)–(21), Eqs. (24)–(25), alongside the boundary conditions (22)–(23), the following equations are obtained

$$D\left(\frac{\partial^2\overline{\vartheta}}{\partial x^2} - g^2\overline{\vartheta}\right) = s(\overline{\vartheta} - \lambda\overline{\theta}) \tag{27}$$

$$\mathfrak{D}\left(1 + \frac{d_T}{k}s\right)\left(\frac{\partial^2\overline{\theta}}{\partial x^2} - g^2\overline{\theta}\right) = s(\overline{\theta} - \varphi\overline{\vartheta}) \tag{28}$$

$$\overline{\theta}\,|_{x=0} = 0,\ \overline{\theta}\,|_{x=a} = \frac{\theta_1}{t_0}\left(\frac{1 - e^{-t_0 s}}{s^2}\right) = G_1(s) \tag{29}$$

$$\overline{\vartheta}\,|_{x=0} = 0,\ \overline{\vartheta}\,|_{x=a} = \frac{\vartheta_1}{t_0}\left(\frac{1 - e^{-t_0 s}}{s^2}\right) = G_2(s) \tag{30}$$

$$\overline{T}(x, z, s) = \overline{\theta}(x, s)\sin(gz) \tag{31}$$

$$\overline{C}(x, z, s) = \overline{\vartheta}(x, s)\sin(gz) \tag{32}$$

A finite Fourier sine transform [40] is defined by

$$\overline{f}_s(m) = F\{f(x)\} = \int_0^a f(x)\,\sin(qx)\,\mathrm{d}x,\ q = m\pi/a \tag{33}$$

with its inverse Fourier sine transform

$$f(x) = F^{-1}\{\overline{f}_s(m)\} = \frac{2}{a}\sum_{m=1}^{\infty}\overline{f}_s(m)\sin(qx) \tag{34}$$

Eqs. (33) and (34) can be used to solve the previously stated Eqs. (27) and (28), using the operational property [40]

$$F\left\{\frac{\mathrm{d}^2 f(x)}{\mathrm{d}x^2}\right\} = -q^2\overline{f}_s(m) + q[f(0) - (-1)^m f(a)] \tag{35}$$

The governing Eqs. (27)–(28), and keeping in mind the boundary conditions (29)–(30) and using the operational property given in Eq. (35), can be depicted in the following ways

$$\overline{\overline{\theta}} = \frac{s\varphi\overline{\overline{\vartheta}} + (-1)^{m+1}\mathfrak{D}q\, G_1(s)G_3(s)}{\mathfrak{D}G_3(s)(q^2+g^2)+s} \tag{36}$$

$$\overline{\overline{\vartheta}} = \frac{s\lambda\overline{\overline{\theta}} + Dq\,(-1)^{m+1}G_2(s)}{D(q^2+g^2)+s} \tag{37}$$

where

$$G_3(s) = 1 + (d_T/k)s$$

Solving Eqs. (36) and (37), we obtain

$$\overline{\overline{\theta}} = \frac{(-1)^{m+1}q\{Ds\varphi G_2 + [D(g^2+q^2)+s]\mathfrak{D}G_1G_3\}}{s[D(g^2+q^2)+s] + (g^2+q^2)[D(g^2+q^2)+s]\mathfrak{D}G_3 - s^2\lambda\varphi} \tag{38}$$

$$\overline{\overline{\vartheta}} = \frac{(-1)^{m+1}q\{s\mathfrak{D}\lambda G_1G_3 + DG_2[s+(g^2+q^2)\mathfrak{D}G_3]\}}{s[D(g^2+q^2)+s] + (g^2+q^2)[D(g^2+q^2)+s]\mathfrak{D}G_3 - s^2\lambda\varphi} \tag{39}$$

Then we perform the inverse finite Fourier sine transform to both sides of Eqs. (38) and (39), and we obtain

$$\overline{\theta} = \sum_{m=1}^{\infty} \frac{(-1)^{m+1}2q\{Ds\varphi G_2 + [D(g^2+q^2)+s]\mathfrak{D}G_1G_3\}\sin(qx)}{sa[D(g^2+q^2)+s] + (g^2+q^2)[D(g^2+q^2)+s]\mathfrak{D}G_3 - s^2\lambda\varphi} \tag{40}$$

$$\overline{\vartheta} = \sum_{m=1}^{\infty} \frac{(-1)^{m+1}2q\{s\mathfrak{D}\lambda G_1G_3 + DG_2[s+(g^2+q^2)\mathfrak{D}G_3]\}\sin(qx)}{sa[D(g^2+q^2)+s] + (g^2+q^2)[D(g^2+q^2)+s]\mathfrak{D}G_3 - s^2\lambda\varphi} \tag{41}$$

Substituting Eqs. (40) into (31) and (41) into (32), one obtains

$$\overline{T} = \sum_{m=1}^{\infty} \frac{(-1)^{m+1}2q\{Ds\varphi G_2 + [D(g^2+q^2)+s]\mathfrak{D}G_1G_3\}\sin(qx)\sin(gz)}{sa[D(g^2+q^2)+s] + (g^2+q^2)[D(g^2+q^2)+s]\mathfrak{D}G_3 - s^2\lambda\varphi} \tag{42}$$

$$\overline{C} = \sum_{m=1}^{\infty} \frac{(-1)^{m+1}2q\{s\mathfrak{D}\lambda G_1G_3 + DG_2[s+(g^2+q^2)\mathfrak{D}G_3]\}\sin(qx)\sin(gz)}{sa[D(g^2+q^2)+s] + (g^2+q^2)[D(g^2+q^2)+s]\mathfrak{D}G_3 - s^2\lambda\varphi} \tag{43}$$

The temperature and moisture distribution, as mentioned in Eqs. (42) and (43), are in the Laplace domain, whose inversion has not yet been known analytically due to its complexity. Using a numerical technique based on Riemann-sum approximation is a very efficient transition from Laplace domain to time domain (Refer to Sect. 5).

In the same way, when we apply the Laplace transform defined in Eq. (26) into Eqs. (12) through (16), we obtain

$$EI\frac{\partial^4\overline{w}}{\partial x^4} + \rho A\, s^2\overline{w} + \frac{\partial^2\overline{M}_c}{\partial x^2} = 0 \tag{44}$$

$$\overline{w}\,|_{x=0} = 0,\ \overline{w}\,|_{x=a} = 0, \tag{45}$$

$$\left.\frac{\partial^2\overline{w}}{\partial t^2}\right|_{x=0} = 0,\ \left.\frac{\partial^2\overline{w}}{\partial t^2}\right|_{x=a} = 0, \tag{46}$$

$$\frac{\overline{\sigma}_x}{E} = -z\frac{\partial^2\overline{w}(x,s)}{\partial x^2} - [\alpha_1(\overline{T}-\overline{T}_0) + \alpha_2(\overline{C}-\overline{C}_0)] \tag{47}$$

$$\overline{M}_c = bE\int_{-h/2}^{h/2}[\alpha_1(\overline{T}-\overline{T}_0) + \alpha_2(\overline{C}-\overline{C}_0)]\,z\,dz \tag{48}$$

On simplification of Eq. (48), one obtains

$$\overline{M}_c = \sum_{m=1}^{\infty} \frac{\begin{array}{c}(-1)^{1+m} q\{\mathfrak{D}[D(g^2+q^2)\alpha_1 + s(\alpha_1+\alpha_2\lambda)]G_1G_3 \\ +DG_2[s(\alpha_2+\alpha_1\varphi)+(g^2+q^2)\mathfrak{D}\alpha_2G_3]\}\end{array}}{s[D(g^2+q^2)+s-s\lambda\varphi]+(g^2+q^2)[D(g^2+q^2)+s]\mathfrak{D}G_3} \times \frac{2bE\sin(qx)}{ag^2}\left[-gh\cos\left(\frac{gh}{2}\right)+2\sin\left(\frac{gh}{2}\right)\right] \tag{49}$$

Recalling the following operational property [40] of finite Fourier sine transform

$$F\left\{\frac{\mathrm{d}^4 f(x)}{\mathrm{d}x^4}\right\} = q^4\overline{f}_s(m) - q^3[f(0)+(-1)^{m+1}f(a)] + q\left[\frac{\mathrm{d}^2 f(0)}{\mathrm{d}x^2} - (-1)^m\frac{\mathrm{d}^2 f(a)}{\mathrm{d}x^2}\right] \tag{50}$$

Applying the finite Fourier sine transform defined in Eq. (34) on both sides of Eq. (44) and using boundary conditions (45)–(46), with the help of the operational property given by Eqs. (50) and then taking its inversion, we obtain

$$\overline{w} = \sum_{m=1}^{\infty} \frac{\begin{array}{c}(-1)^{1+m} q^3\{\mathfrak{D}[D(g^2+q^2)\alpha_1 + s(\alpha_1+\alpha_2\lambda)]G_1G_3 \\ +DG_2[s(\alpha_2+\alpha_1\varphi)+(g^2+q^2)\mathfrak{D}\alpha_2G_3]\}\end{array}}{s\,[D(g^2+q^2)+s-s\lambda\varphi]+(g^2+q^2)[D(g^2+q^2)+s]\mathfrak{D}G_3} \times \frac{2bE\sin(qx)}{ag^2(EIq^4+\rho As^2)}\left[-gh\cos\left(\frac{gh}{2}\right)+2\sin\left(\frac{gh}{2}\right)\right] \tag{51}$$

Substituting Eqs. (51) and (42)-(43) into Eqs. (47), one obtains the $\overline{\sigma}_x$ under hygrothermal loading in the Laplace domain. Upon the determination of $\overline{w}$ and $\overline{\sigma}_x$, the final numerical results can be obtained by employing the inverse Laplace transform using the Riemann-sum approximation method.

5 Numerical inversion of the Laplace transform

The Riemann-sum approximation method [20] is used to get the numerical results and determine the solutions in the time domain. In this numerical approach, any function that exists in the Laplace domain (s-domain) can be converted to a time domain (t-domain) as follows:

$$f(t) = \frac{e^{\hat{k}t}}{t}\left[\frac{1}{2}\overline{f}(\hat{k}) + \mathrm{Re}\sum_{n=1}^{N}(-1)^n\overline{f}\left(\hat{k}+\frac{in\pi}{t}\right)\right] \tag{52}$$

where i is an imaginary number unit, Re is the real part, n is the number of terms used in the Riemann-sum approximation, and $\hat{k}$ is the real part of the Bromwich contour that is used in inverting. Numerous computational studies have demonstrated that the value of $\hat{k}$ meets the relation $\hat{k}t \approx 4.7$ for faster convergence.

6 Numerical result and discussion

In this section, in order to obtain the numerical results, we introduce the non-dimensional variables listed below for simplification [39]

$$\begin{aligned} &\overline{x} = x/a,\ \overline{z} = z/h,\ \overline{h} = h/a,\ \overline{w} = w/h \\ &\overline{T} = \frac{T-T_0}{T_0},\ \overline{C} = \frac{C-C_0}{\psi T_0},\ \tau = (c/a)t, \\ &c^2 = E/\rho,\ \overline{\sigma}_x = \sigma_x/E \end{aligned} \tag{53}$$

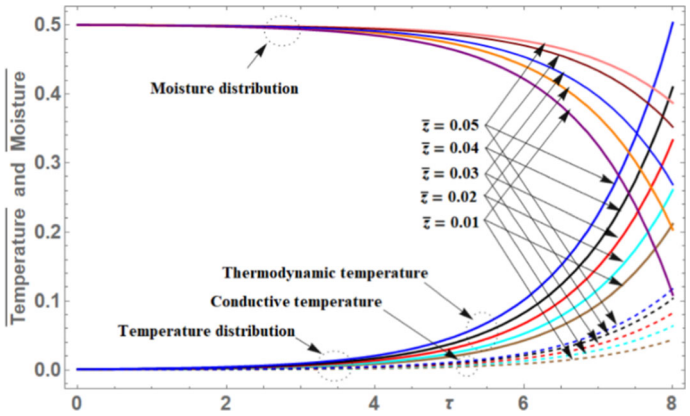

Fig. 2 The temperature and moisture distribution along τ for various $\bar{z}$

Baggio et al. [41] designed a model to represent the procedure of heat and mass transfer that occurs in a porous medium from the macroscopic point of view. Here Clapeyron's and Kelvin's equations are derived, letting the equilibrium evolve through different paths during modeling moisture transfer and phase change in a porous media.

Gawin et al. [42] considered concrete as a multi-phase porous visco-elastic material in which nonlinearities with temperature, moisture content, and the maturity of concrete (hydration degree) have been taken into account using a finite element model. These phase changes include adsorption–desorption, evaporation—condensation, chemical reactions (hydration), different fluid flows, and phase changes with temperature. The literature review [41, 42] observed that a detailed study was conducted with phase change and chemical effects for macroscopic porous media. Taking the above research for granted, the author intends to take the porous composite material in a non-simple nano-beam subjected to hygrothermal loading. The hygrothermoelastic distribution of a beam is calculated numerically for a porous composite material with material properties [1]

$$\begin{gathered}\alpha_1 = 31.3 \times 10^{-6}\,\mathrm{cm/(cm\,^oC)},\ \alpha_2 = 2.68 \times 10^{-3}\,\mathrm{cm/(cm\,\%\,H_2O)},\\ \varphi = 0.5\,\mathrm{cm^3\,^oC/g},\ \psi = 0.5\,g/(\mathrm{cm\,^oC}),\ \mathfrak{D} = 2.16 \times 10^{-5}\,\mathrm{m^2/s},\\ D = 2.16 \times 10^{-6}\,\mathrm{m^2/s},\ \rho = 1590\,\mathrm{kg/m^3},\ E = 64.3\ \mathrm{GPa},\ \upsilon = 0.33.\end{gathered} \tag{54}$$

Taking fixed aspect ratios as $a/h = 10$, $b/h = 1/2$ and $d_T = 1.2$. When h is varied, a and b changed accordingly with h. For the nanoscale beam, we will take the range of beam length a $(1-100) \times 10^{-12}$ m. The original time t and the ramping time parameter t_0 will be considered in the picoseconds $(1-100) \times 10^{-14}$ sec. The figures were prepared by using the non-dimensional variables defined in Eq. (53) for a wide range of beam length when $a = 1, z = h/6$ and $t = 0.15$. Figures 2 through 14 show the different variations of dimensionless thermal and moisture distribution, plate deflection, and stress caused by hydrothermal loading on the plate. The transient temperature fields of thermodynamic and conductive temperatures with the coupled case are depicted in Figs. 2 through 4, representing solid lines and dashed lines, respectively.

From Fig. 2, we can see that for thermal and moisture diffusion behavior, the dimensionless temperature (i.e., thermodynamic temperature and conductive temperature) when the hygrothermal coupling is taken into account is always higher than that without the hygrothermal coupling along the time direction at various points of $\bar{z}$. This is because the hygrothermal coupling allows the thermodynamic temperature and the conductive temperature to be calculated more accurately. If the moisture rate $(\partial\overline{C}/\partial t > 0)$ is positive, then the moisture functions act as a heat source for the temperature distribution, and if the moisture rate $(\partial\overline{C}/\partial t < 0)$ is negative, then the moisture function acts as a heat sink. Both of these roles are based on the physical properties of the moisture. The result agrees with the conclusion drawn from the earlier study [10]. Figure 3 shows the variation in the thermodynamic and conductive temperature for various locations in the points along the radial direction, which depends on the time and space coordinate and the two-temperature parameter b. The value of $d_T = 0$ indicates the one-temperature theory, while $d_T \neq 0$ indicates the two-temperature theory. The variation in the thermodynamic and conductive temperature along the radial direction may be due to the available sectional heat source. The plate's temperature reaches its highest point at $\bar{x} = 0$, and while it is maintained at 0 degrees Celsius, the temperature gradually decreases as it moves toward $\bar{x} = b$. The findings are consistent with the previously [43] obtained information.

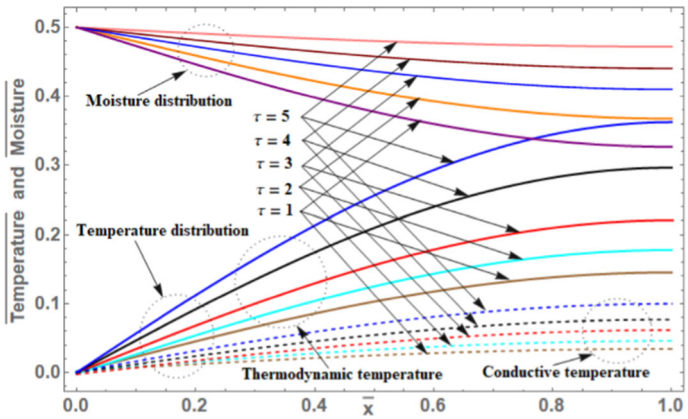

Fig. 3 The temperature and moisture distribution along $\overline{x}$ for various τ

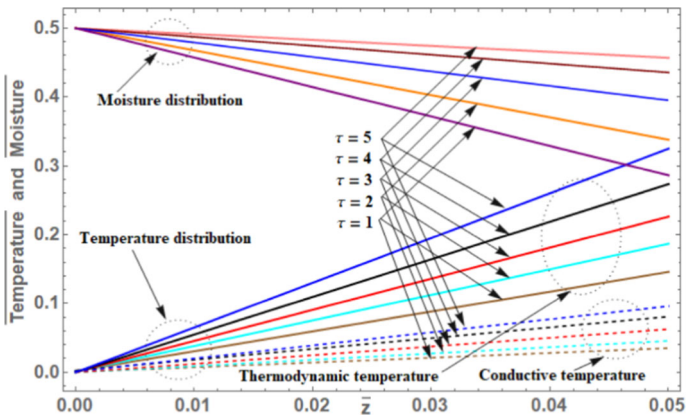

Fig. 4 The temperature and moisture distribution along $\overline{z}$ for various τ

Figure 4 illustrates the temperature and moisture distribution in the axial direction at a series of dimensionless times. If the hygrothermal coupling is neglected, it is evident that there will never be any moisture on the surface, just as was predicted, because no moisture will be supplied to the surface. The hygrothermal coupling theory concludes that temperature shifts are the sole agents responsible for the movement of moisture throughout an environment. It has been noticed that as one moves closer to the heated zone in the thin plate, both temperatures and levels of moisture slope linearly. This may be because the width of the plate is so narrow. The reported results are comparable in nature to those found for the thermodynamic temperature [44], which were derived from physically equivalent assumptions. It can be seen quite clearly from Figs. 2, 3 and 4 that the dimensionless temperature starts from the origin, and significant variation was found near the outer surface along x and z. This could be because there is a sectional heat supply available; similarly, the moisture has a rapid response near the surface. As a result, the moisture field directly relies on the temperature change ratio.

Figure 5 illustrates the change in the dimensionless deflection profile that occurs with an increase in the time span τ for a variety of $\overline{x}$ values. The magnitude of the plate's deflection can increase toward the plate's periphery and reach its maximum value when $\overline{x}$ it is equal to one unit, as was to be anticipated.

Figure 6 depicts the dimensionless thermal deflection along $\overline{x}$ for a range of different values of the dimensionless time τ. It has been found that the region near the center of the plate experiences a tremendous amount of tensile stress, which is in agreement with Eq. (14).

The coupled thermal deflection in isolines contour plot along $\overline{x}$ and $\overline{z}-$ directions at a fixed temperature discrepancy factor $d_T = 1.2$ and dimensionless time τ can be seen by looking at Fig. 7. The darkly shaded plot portion agrees with the graph plotted in Fig. 2, which can be seen by looking at Fig. 7. The highest displacement can be seen in the red area close to the plate's outside edge. This could be because of the sectional heat supply. In contrast, the deflection is at a standstill in the blue area in the plate's middle.

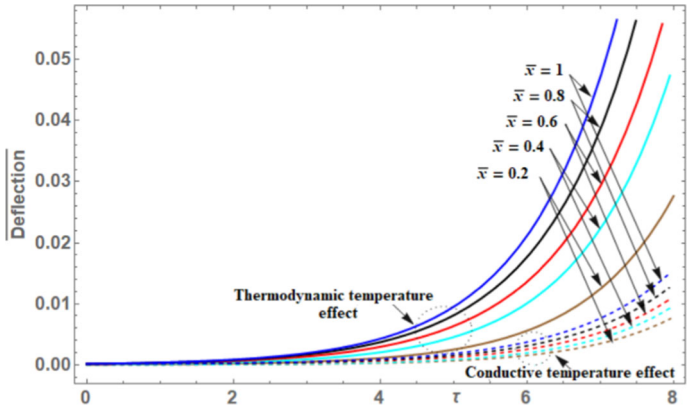

Fig. 5 The thermal deflection along τ for various $\overline{x}$

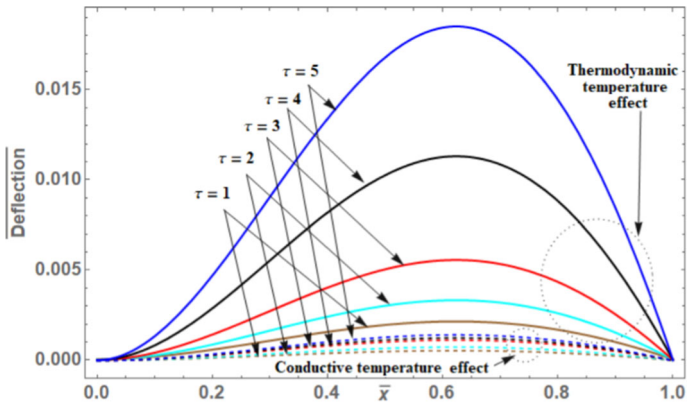

Fig. 6 The thermal deflection along $\overline{x}$ for various τ

The dimensionless thermal stress along the τ axis is depicted in Fig. 8 for various locations of $\overline{x}$. This illustrates that a greater amount of compressive stress is taking place at the inner radius, which continues to increase along the τ-direction until it reaches its highest point at the outer edge.

Figure 9 depicts the change in the dimensionless strains that are present in a plate along $\overline{x}$ for each of the different τ values. The stress components are compressive toward the origin, but the maximal tensile force is acting toward the outer surface as a result of the accumulation of thermal energy that was dissipated by the sectional supply.

Figure 10 depicts the dimensionless thermal stress along $\overline{z}$ for a variety of time spans denoted by τ. It can be seen from the graphic that the stress along the time axis experiences a linear increase from 0 to positive values for a range of $\overline{z}$ values. An increase in the rate of heat propagation, which at first causes a compressive force and then expands further as time passes, could be the cause of an increment in the level of stress.

The result in Fig. 11 also shows the variation in the temperature distribution for various locations along the $\overline{x}$ direction and on time for different values of temperature discrepancy factor is $d_T = 0,\ 0.5,\ 0.7,\ 1.1,$ 2.2. The value $d_T = 0$ indicates the one-temperature theory. In contrast, $d_T = 0.5,\ 0.7,\ 1.1,\ 2.2$ shows the two-temperature approach. The maximum temperature occurs at the outer edge of the plate due to the available uniform sectional heat supply. The result agrees with the previous results [43].

7 Conclusion

This hygrothermal model was examined with the aid of the integral transform methodology, which consists of the Laplace transform and the finite Fourier sine transform method. The closed-form solution is obtained to describe the effects of coupled temperature and moisture on a non-simple nano-beam subjected to hygrothermal loading. Further, its hygrothermoelastic deflection and stress response was also examined. The numerical results

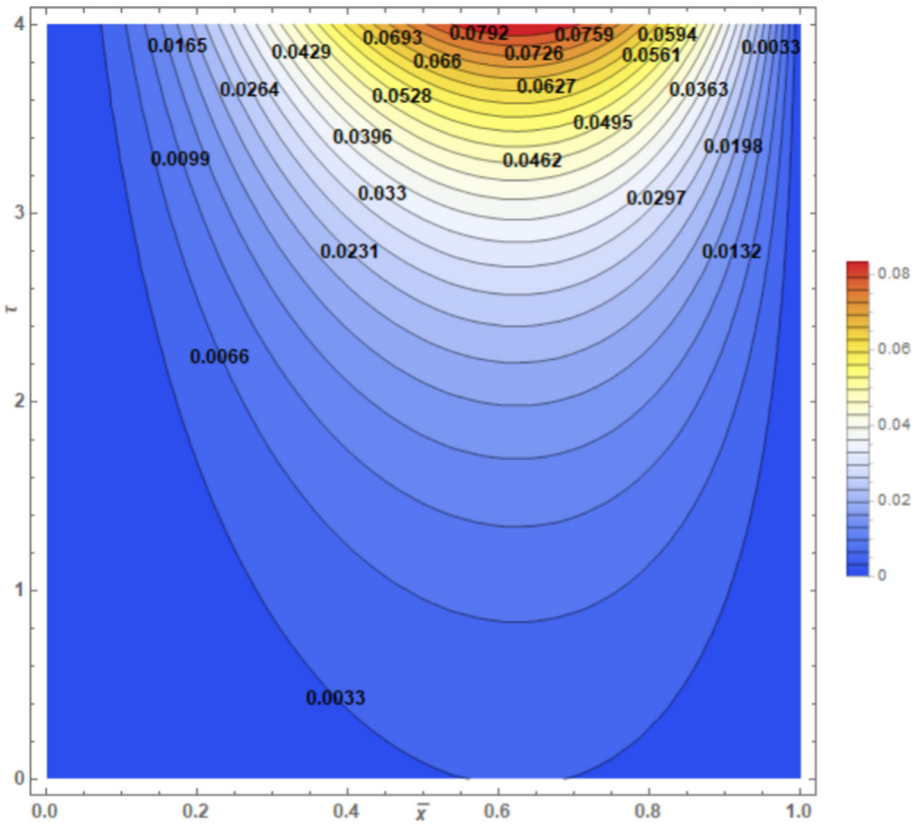

Fig. 7 Contour plot of deflection along $\overline{x}\overline{z}$-plane for a fixed value of τ

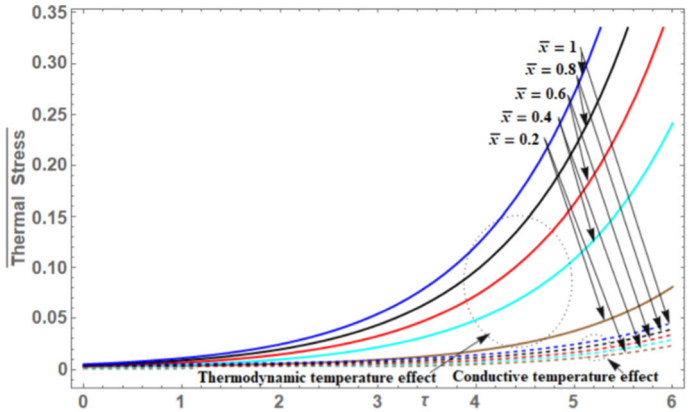

Fig. 8 The stress distribution along τ for various $\overline{x}$

of moisture diffusion and temperature distribution for various parameters have been calculated and illustrated graphically. The numerical results of temperature distribution and moisture diffusion for different parameters have been computed and graphically depicted. This approach can be used to solve problems analytically concerning moisture and temperature distribution.

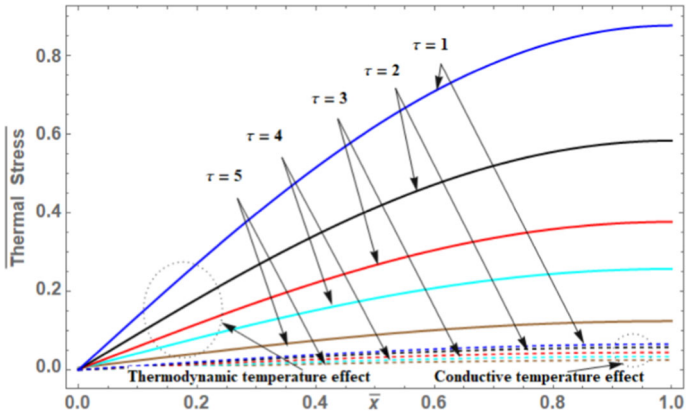

Fig. 9 The stress distribution along $\bar{x}$ for various τ

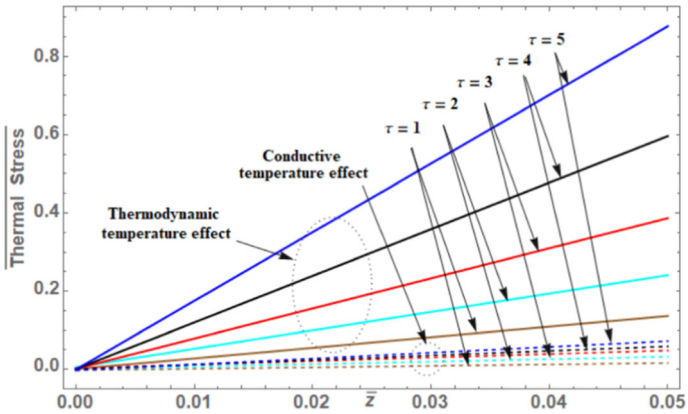

Fig. 10 The stress distribution along $\bar{z}$ for various τ

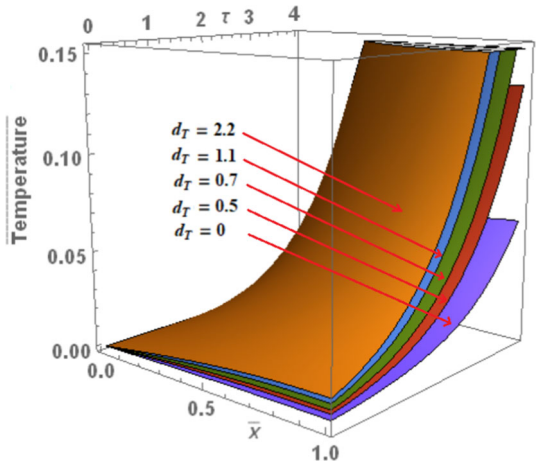

Fig. 11 The temperature distribution along $\bar{x}$ and τ for various b

References

1. Sih, G.C., Michopoulos, J.G., Chou, S.C.: Hygrothermoelasticity. Springer, Dordrecht (1986). https://doi.org/10.1007/978-94-009-4418-3
2. Chang, W.J.: Transient hygrothermal responses in a solid cylinder by linear theory of coupled heat and moisture. Appl. Math. Model. **18**(8), 467–473 (1994). https://doi.org/10.1016/0307-904X(94)90309-3
3. Sugano, Y., Chiba, R.: An analytical solution for hygrothermoelastic problem in a functionally graded material plate and material composition design. In: NCTAM Papers, National Congress of Theoretical and Applied Mechanics, Japan, Vol. 54, pp. 82–82 (2005). https://doi.org/10.11345/japannctam.54.0.82.0
4. Chiba, R., Sugano, Y.: Transient hygrothermoelastic analysis of layered plates with one-dimensional temperature and moisture variations through the thickness. Compos. Struct. **93**, 2260–2268 (2011). https://doi.org/10.1016/j.compstruct.2011.03.014
5. Brischetto, S.: Hygrothermal loading effects in bending analysis of multilayered composite plates. Comput. Model. Eng. Sci. **88**(5), 367–418 (2012). https://doi.org/10.3970/cmes.2012.088.367
6. Ishihara, M., Ootao, Y., Kameo, Y.: Hygrothermal field considering nonlinear coupling between heat and binary moisture diffusion in porous media. J. Therm. Stress. **37**(10), 1173–1200 (2014). https://doi.org/10.1080/01495739.2014.936232
7. Saadatfar, M., Aghaie-Khafri, M.: Hygrothermomagnetoelectroelastic analysis of a functionally graded magnetoelectroelastic hollow sphere resting on an elastic foundation. Smart Mater. Struct. **23**, 0350041–0350113 (2014). https://doi.org/10.1088/0964-1726/23/3/035004
8. Zenour, A.M.: Hygrothermoelastic responses of inhomogeneous piezoelectric and exponentially graded cylinders. Int. J. Press. Vessel. Pip. **119**, 8–18 (2014). https://doi.org/10.1016/j.ijpvp.2014.02.001
9. Zhao, M.H., Dang, H.Y., Fan, C.Y., Chen, Z.T.: Three-dimensional steady-state general solution for isotropic hygrothermoelastic media. J. Therm. Stress **41**(8), 951–972 (2018). https://doi.org/10.1080/01495739.2018.1449040
10. Bhoyar, S., Varghese, V., Khalsa, L.: Hygrothermoelastic response in the bending analysis of elliptic plate due to hygrothermal loading. J. Therm. Stress **43**(3), 372–400 (2020). https://doi.org/10.1080/01495739.2019.1711477
11. Hosseinian, E., Theillet, P.O., Pierron, O.N.: Temperature and humidity effects on the quality factor of a silicon lateral rotary micro-resonator in atmospheric air. Sens. Actuator A Phys. **189**, 380–389 (2013). https://doi.org/10.1016/j.sna.2012.09.020
12. Jan, M.T., Ahmad, F., Hamid, N.H.B., Khir, M.H.B.M., Shoaib, M., Ashraf, K.: Experimental investigation of temperature and relative humidity effects on resonance frequency and quality factor of CMOS-MEMS paddle resonator. Microelectron. Reliab. **63**, 82–89 (2016). https://doi.org/10.1016/j.microrel.2016.05.007
13. Nguyen, C.C., Ngo, V.K.T., Le, H.Q., Li, W.L.: Influences of relative humidity on the quality factors of MEMS cantilever resonators in gas rarefaction. Microsyst. Technol. **25**(7), 2767–2782 (2018). https://doi.org/10.1007/s00542-018-4239-x
14. Jouneghani, F.Z., Dimitri, R., Tornabene, F.: Structural response of porous FG nano-beams under hygro-thermo-mechanical loadings. Compos. B. Eng. **152**, 71–78 (2018). https://doi.org/10.1016/j.compositesb.2018.06.023
15. Eichler, A., Moser, J., Chaste, J., Zdrojek, M., Wilson-Rae, I., Bachtold, A.: Nonlinear damping in mechanical resonators made from carbon nanotubes and graphene. Nat. Nanotechnol. **6**(6), 339–342 (2011). https://doi.org/10.1038/nnano.2011.71
16. Ebrahimi, F., Barati, M.R.: Hygrothermal effects on static stability of embedded single-layer graphene sheets based on nonlocal strain gradient elasticity theory. J. Therm. Stress. **42**(12), 1535–1550 (2019). https://doi.org/10.1080/01495739.2019.1662352
17. Kumar, H., Mukhopadhyay, S.: Thermoelastic damping in micro and nanomechanical resonators utilizing entropy generation approach and heat conduction model with a single delay term. Int. J. Mech. Sci. **165**, 105211 (2020). https://doi.org/10.1016/j.ijmecsci.2019.105211
18. Youssef, H.M., El-Bary, A.A., Al-Lehaibi, E.A.N.: Characterisation of the quality factor due to the static prestress in classical Caputo and Caputo-Fabrizio fractional thermoelastic silicon microbeam. Polym. J. **13**(1), 27 (2020). https://doi.org/10.3390/polym13010027
19. Zhang, X.Y., Peng, Y., Xie, Y.J.: Hygrothermoelastic response of a hollow cylinder based on a coupled time-fractional heat and moisture transfer model. Z. Angew. Math. Phys. **70**(2), 1–21 (2019). https://doi.org/10.1007/s00033-018-1047-1
20. Tzou, D.: Marco-to-micro heat transfer. Taylor & Francis, Washington, DC (1996). https://doi.org/10.1002/9781118818275
21. Lord, H.W., Shulman, Y.: A generalized dynamical theory of thermoelasticity. J. Mech. Phys. Solids **15**(5), 299–309 (1967). https://doi.org/10.1016/0022-5096(67)90024-5
22. Tzou, D.Y.: A unified field approach for heat conduction from macro- to micro-scales. J. Heat Transf. **117**(1), 8–16 (1995). https://doi.org/10.1115/1.2822329
23. Povstenko, Y.: Fractional Thermoelasticity, vol. 219. Springer, Berlin (2015). https://doi.org/10.1007/978-3-319-15335-3
24. Sun, Y., Fang, D., Saka, M., Soh, A.K.: Laser-induced vibrations of micro-beams under different boundary conditions. Int. J. Solids Struct. **45**, 1993–2013 (2008). https://doi.org/10.1016/j.ijsolstr.2007.11.006
25. Soh, A.K., Sun, Y., Fang, D.: Vibration of microscale beam induced by laser pulse. J. Sound Vib. **311**, 243–253 (2008). https://doi.org/10.1016/j.jsv.2007.09.002
26. Youssef, H.M., Elsibai, K.A.: Vibration of nano-beam induced by ramp type heating. World J. Nano Sci. Eng. **1**, 37–44 (2011). https://doi.org/10.4236/wjnse.2011.12006
27. Andarwa, S., Tabrizi, H.B.: Non-Fourier effect in the presence of coupled heat and moisture transfer. Int. J. Heat Mass Transf. **53**(15–16), 3080–3087 (2010). https://doi.org/10.1016/j.ijheatmasstransfer.2010.03.019
28. Silva, F.R.G.B., Gonçalves, G., Lenzi, M.K., Lenzi, E.K.: An extension of the linear Luikov system equations of heat and mass transfer. Int. J. Heat Mass Transf. **63**, 233–238 (2013). https://doi.org/10.1016/j.ijheatmasstransfer.2013.04.007
29. Ezzat, M.A., Othman, M.I., Smaan, A.A.: State space approach to two-dimensional electromagneto–thermoelastic problem with two relaxation times. Int. J. Eng. Sci. **39**(12), 1383–1404 (2001). https://doi.org/10.1016/S0020-7225(00)00095-1
30. El-Karamany, A.S., Ezzat, M.A.: Thermoelastic diffusion with memory-dependent derivative. J. Therm. Stress. **39**(9), 1035–1050 (2016). https://doi.org/10.1080/01495739.2016.1192847

31. Hosseini, S.M., Rad, M.H.G.: Application of meshless local integral equations for two-dimensional transient coupled hygrothermoelasticity analysis: moisture and thermoelastic wave propagations under shock loading. J. Therm. Stress. **40**(1), 40–54 (2016). https://doi.org/10.1080/01495739.2016.1224134
32. Peng, Y., Zhang, X.Y., Li, X.F.: Effect of phase lags of moisture–heat flow on the hygrothermoelastic field of hollow cylinders with convective surfaces. Mech. Based Des. Struct. Mach. **51**(6), 3004–3025 (2021). https://doi.org/10.1080/15397734.2021.1914654
33. Xue, Z., Tian, X., Liu, J.: Non-classical hygrothermal fracture behavior of a hollow cylinder with a circumferential crack. Eng. Fract. Mech. **224**, 106805 (2020). https://doi.org/10.1016/j.engfracmech.2019.106805
34. Zhang, X.Y., Li, X.F.: Transient response of hygrothermoelastic field in an elastic plate with an edge crack. Z. Angew. Math. Phys. **100**(9), e202000005 (2020). https://doi.org/10.1002/zamm.202000005
35. Henry, P.S.H.: Diffusion in absorbing media. Proc. R. Soc. Lond. A **171**, 215–241 (1939). https://doi.org/10.1098/rspa.1939.0062
36. Chen, P.J., Gurtin, M.E.: On a theory of heat conduction involving two temperatures. Z. Angew. Math. Phys. **19**, 614–627 (1968). https://doi.org/10.1007/BF01594969
37. Chen, P.J., Gurtin, M.E., Willams, W.O.: On the thermodynamics of non-simple elastic material with two temperatures. Z. Angew. Math. Phys. **20**, 107–112 (1969). https://doi.org/10.1007/BF01591120
38. Lifshitz, R., Roukes, M.L.: Thermoelastic damping in micro- and nanomechanical systems. Phys. Rev. B **61**(8), 5600–5609 (2000). https://doi.org/10.1103/PhysRevB.61.5600
39. Zhang, X.Y., Li, X.F.: Hygrothermoelastic damping of beam resonators with non-Fourier and non-Fick effects. Thin Walled Struct. **168**, 108283 (2021). https://doi.org/10.1016/j.tws.2021.108283
40. Debnath, L., Bhatta, D.: Integral Transforms and their Applications. Chapman and Hall/CRC, New York (2006). https://doi.org/10.1201/9781420010916
41. Baggio, P., Bonacina, C., Schefler, B.A.: Some considerations on modeling heat and mass transfer in porous media. Transp. Porous Media **28**, 233–251 (1997). https://doi.org/10.1023/A:1006525729566
42. Gawin, D., Pesavento, F., Schrefler, B.A.: Hygro-thermo-chemo-mechanical modelling of concrete at early ages and beyond Part I Hydration and hygro-thermal phenomena. Int. J. Numer. Methods Eng. **67**(3), 299–331 (2006). https://doi.org/10.1002/nme.1615
43. Zenkour, A.M., Abouelregal, A.E.: Non-simple magneto-thermoelastic solid cylinder with variable thermal conductivity due to harmonically varying heat. Earthq. Struct. **10**(3), 681–697 (2016). https://doi.org/10.12989/eas.2016.10.3.681
44. Benkhedda, A., Tounsi, A., Adda bedia, E.A.: Effect of temperature and humidity on transient hygrothermal stresses during moisture desorption in laminated composite plates. Compos. Struct. **82**(4), 629–635 (2008). https://doi.org/10.1016/j.compstruct.2007.04.013